JACS Au
AN OPEN ACCESS JOURNAL OF THE AMERICAN CHEMICAL SOCIETY

pubs.acs.org/jacsau Article

Understanding the Solvation-Dependent Properties of Cyclic Ether Multivalent Electrolytes Using High-Field NMR and Quantum Chemistry

Jian Zhi Hu,*[,‖] Nicholas R. Jaegers,[‖] Nathan T. Hahn,* Wenda Hu, Kee Sung Han, Ying Chen, Jesse A. Sears, Vijayakumar Murugesan, Kevin R. Zavadil, and Karl T. Mueller*

Cite This: *JACS Au* 2022, 2, 917−932 Read Online

ACCESS | Metrics & More | Article Recommendations | Supporting Information

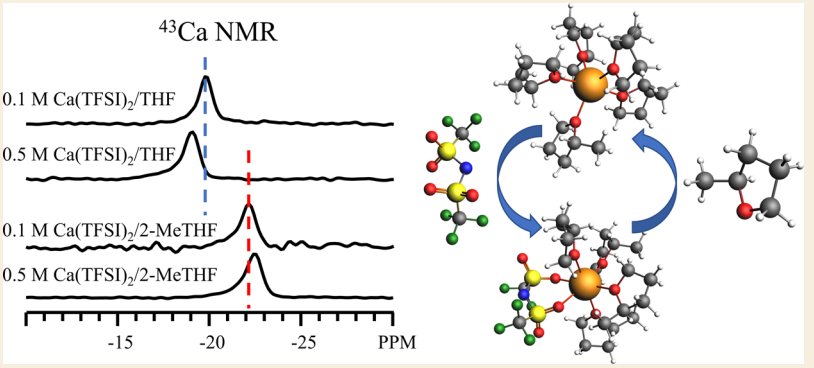

ABSTRACT: Efforts to expand the technological capability of batteries have generated increased interest in divalent cationic systems. Electrolytes used for these electrochemical applications often incorporate cyclic ethers as electrolyte solvents; however, the detailed solvation environments within such systems are not well-understood. To foster insights into the solvation structures of such electrolytes, $Ca(TFSI)_2$ and $Zn(TFSI)_2$ dissolved in tetrahydrofuran (THF) and 2-methyl-tetrahydrofuran were investigated through multi-nuclear magnetic resonance spectroscopy (^{17}O, ^{43}Ca, and ^{67}Zn NMR) combined with quantum chemistry modeling of NMR chemical shifts. NMR provides spectroscopic fingerprints that readily couple with quantum chemistry to identify a set of most probable solvation structures based on the best agreement between the theoretically predicted and experimentally measured values of chemical shifts. The multi-nuclear approach significantly enhances confidence that the correct solvation structures are identified due to the required simultaneous agreement between theory and experiment for multiple nuclear spins. Furthermore, quantum chemistry modeling provides a comparison of the solvation cluster formation energetics, allowing further refinement of the preferred solvation structures. It is shown that a range of solvation structures coexist in most of these electrolytes, with significant molecular motion and dynamic exchange among the structures. This level of solvation diversity correlates with the solubility of the electrolyte, with $Zn(TFSI)_2$/THF exhibiting the lowest degree of each. Comparisons of analogous Ca^{2+} and Zn^{2+} solvation structures reveal a significant cation size effect that is manifested in significantly reduced cation−solvent bond lengths and thus stronger solvent bonding for Zn^{2+} relative to Ca^{2+}. The strength of this bonding is further reduced by methylation of the cyclic ether ring. Solvation shells containing anions are energetically preferred in all the studied electrolytes, leading to significant quantities of contact ion pairs and consequently neutrally charged clusters. It is likely that the transport and interfacial de-solvation/re-solvation properties of these electrolytes are directed by these anion interactions. These insights into the detailed solvation structures, cation size, and solvent effects, including the molecular dynamics, are fundamentally important for the rational design of electrolytes in multivalent battery electrolyte systems.

KEYWORDS: *divalent batteries, electrolytes, tetrahydrofuran, natural abundance ^{17}O, ^{43}Ca and ^{67}Zn NMR, and DFT calculations*

INTRODUCTION

Understanding and advancing the systems available for energy storage represent a topic of immense interest due to a growing economic and technical demand for larger capacity, durable battery cells. Rechargeable Li-ion batteries dominate the market as state of the art in terms of energy capacity and long-term stability; however, the present formulation is

Received: January 25, 2022
Revised: February 22, 2022
Accepted: March 1, 2022
Published: March 21, 2022

https://doi.org/10.1021/jacsau.2c00046
JACS Au 2022, 2, 917−932

insufficient to meet the needs of more energy-intensive technologies which have sparked the demand for improved battery performance standards and necessitate refined electrochemical cell formulation. These efforts have been directed at divalent cation systems such as Mg^{2+} and Ca^{2+} due to their theoretically higher energy density compared to the Li-ion technology.[1] Further, divalent Zn^{2+} is perceived to be an attractive alternative to Li^{+} for economic and environmental reasons.[2] The stronger interactions between the divalent cations and their environments result in relatively higher de-solvation barriers, necessitating a new regime of electrolyte compositions and renewed efforts to characterize novel battery formulations. Indeed, magnesium-based batteries have attracted attention in recent scientific efforts since understanding the underlying mechanisms behind their performance limitations may lead to the development of a viable material.[3−6]

One feature of batteries that plays an important role in electrochemical performance is that of the electrolyte composition. Electrolytes are important components responsible for transferring active ions between the electrode surfaces during electrochemical cycling as well as directing the formation and composition of the solid−electrolyte interphase. Aside from the selection of cations, whose size may play a role in directing the solvation structures, the anions and solvents employed also have a direct role in the bonding environment, that is, the solvation structures, and thus Coulombic interactions. The inclusion of various cyclic ethers, such as tetrahydrofuran (THF), has been shown to modulate the properties of electrolytes. The structure of THF can be tuned through methylation to 2-methyl-tetrahydrofuran (2-MeTHF), imparting new chemical properties which have been shown to improve electrolyte stability when in contact with acids and reactive metals in Li-based systems. The methylated cyclic ether is sometimes considered to be a favorable hybrid solvent between THF and dialkyl ethers in terms of polarity and Lewis base strength.[7,8] Use of 2-MeTHF has also improved the solubility of Mg-based halides and TFSI salts.[8,9] Breakthroughs in Mg^{2+} cation utilization have extensively employed THF as the solvent due to favorable reductive stability, coordination of cations, and tendency for Mg^{2+} deposition from complexes such as $Mg_2Cl_3^{+}$.[10−15] Such effects also appear to apply when other divalent cations are present. For example the first high-efficiency Ca^{2+} electrolyte ($Ca(BH_4)_2$/THF) utilized THF.[16] Therefore, 2-MeTHF might also be utilized successfully as a multivalent battery solvent if its solvating properties can be understood and controlled. Given the importance of cyclic ethers in the quest to improve advanced battery materials, understanding the interactions between THF and 2-MeTHF and the ions present in divalent cation electrolyte solutions will provide important structure−property correlations to guide future development.

To understand how the ligand substitution of the cyclic ether and cation size impact the solvation structure and performance of the electrolyte systems, detailed characterizations of the interactions between solvent molecules, cations, and anions are required. Studies investigating the unique properties of Ca^{2+} have shown the role of the solvent structure and concentration in controlling the coordination strength, ion transport, and electrochemical performance.[17−19] These results demonstrate the need to deeply characterize how the solvent and anion, both of which impact the cation coordination and performance, interact with the cation in the electrolyte. Toward this goal, we recently investigated the ion interactions present in $Ca(TFSI)_2$ and $Zn(TFSI)_2$ electrolytes dissolved in ether and glyme solvents, finding significant correlations between these interactions and electrolyte transport properties.[19] Despite containing the same anions, we found that these electrolytes exhibit a surprisingly large variation in solubility behavior in cyclic ethers, which is a critical property determining the electrolyte utility. To illustrate, $Zn(TFSI)_2$ is scarcely soluble in THF (~0.004 M) but freely soluble in 2-MeTHF (≥0.5 M), while $Ca(TFSI)_2$ is freely soluble in either solvent. Furthermore, these electrolyte examples yielding high solubility were shown to vary in ionic conductivity by nearly 2 orders of magnitude. Raman analysis indicated that significant contact ion pair (CIP) populations exist in each of these electrolytes, suggesting that more nuanced details of the first shell cation−anion interactions determine both their solubility and transport behaviors.[19] Our prior studies mainly illustrated that anions coordinate more readily with divalent cations in cyclic ethers than in glymes, and the coordination of the anions with Ca^{2+} is more pronounced than with Zn^{2+} in a glyme solvent due to the cation size effect.[19] Although this prior work showed the relation between salt dissociation and the transport properties of electrolytes, it only estimated the average, ensemble solvation structures by providing a percentage of uncoordinated $TFSI^{-}$ anions for each sample without describing the detailed solvation structures. The specific cation size effects among cyclic ethers, including the methyl substitution effects, are also unknown. In the present work, we use multi-nuclear NMR as a nondestructive technique that is nonperturbative to the electronic environment to be analyzed, capable of isotopically specific analysis of the electronic environments of electrolyte constituents. NMR has found profound use in the field of electrochemical energy storage and serves as an important tool for characterizing the electrodes, solid electrolyte interphases, and the electrolytes.[20,21] The custom-built NMR probe employed herein enables detection of low-concentration ionic solutions at natural abundances that are not generally possible on commercial systems.[22−24] Indeed, we have previously used this technique to successfully study various Mg^{2+} systems,[5,6,19,20,25,26] and in this work, we broaden this knowledge base by focusing on two less-well-studied multivalent electrolyte cations due to the relatively challenging and resource-intensive nature of their NMR-active isotopes, Ca^{2+}, whose NMR-active ^{43}Ca nucleus exhibits a low natural abundance of 0.135% and a sensitivity nearly 6 orders of magnitude lower than ^{1}H, and Zn^{2+} whose NMR-active ^{67}Zn nucleus exhibits a natural abundance of 4.1% and a sensitivity that is 4 orders of magnitude lower than ^{1}H. To accomplish this, we employ multinuclear natural abundance (^{17}O, natural abundance of 0.038%; ^{43}Ca; and ^{67}Zn) NMR of these quadrupolar nuclei coupled with quantum chemistry-predicted chemical shifts, including quantum chemical comparisons of solvation structure energetics. Together these techniques demonstrate the complex solvation structures of Ca^{2+} and Zn^{2+} battery electrolyte systems, revealing the effects of cation size and solvent structures. Ligand substitution and salt concentration are also shown to modulate the coordinating ability of the solvent molecules with important ramifications for solubility, conductivity, and de-solvation properties. The detection and interpretation of such solvent−cation−anion interactions have direct implications on the choice and performance of solvents in a battery system.

https://doi.org/10.1021/jacsau.2c00046
JACS Au 2022, 2, 917−932

EXPERIMENTAL METHODS

Sample Preparation

Electrolytes of 0.8 mM to 0.5 M $X(TFSI)_2$ (X = Ca, Zn) in THF and 2-MeTHF were prepared in an argon-filled glovebox as follows: quantities of the divalent X-$(TFSI)_2$ (Solvionic, 99.5%, dried under vacuum at 170 °C) were added to each solvent (Millipore-Sigma, 99% +, anhydrous) at room temperature and allowed to fully dissolve. Final concentrations were determined from the total solution volume. Both salts are highly soluble in 2-MeTHF, but only $Ca(TFSI)_2$ is highly soluble in THF. The saturated concentration of $Zn(TFSI)_2$ in THF was determined at approximately 4 mM. We note that the commercially available $Zn(TFSI)_2$ contains a small amount of insoluble material regardless of the solvent used, but this finely suspended material is visually distinct from undissolved $Zn(TFSI)_2$. About 3.0 mL of each electrolyte solution was sealed in a commercially available clear glass vial measuring 34.9 × 14.3 mm in diameter, where sealing was achieved *via* a polytetrafluoroethylene (PTFE)-lined rubber liner within the cap that was augmented by applying PTFE tape to the vial threads. The vials containing the electrolyte samples were then directly placed inside the 15 mm internal-diameter large-sample-volume probe for the NMR measurement (see below).

Natural Abundance NMR Spectroscopy

^{17}O, ^{67}Zn, and ^{43}Ca NMR experiments were performed using a Varian 850 MHz NMR spectrometer equipped with a custom 15 mm diameter large sample volume probe where the advantages of the significantly increased sensitivity from the use of the combined high magnetic field and larger-sample volume allow for NMR detection of low-concentration species at a natural abundance.[23] The corresponding Larmor frequencies (f) and NMR parameters for the nuclei probed are shown in Table 1, where f is the spectrometer frequency, a_t is the acquisition time of each transient, and d_1 is the recycle delay. Recycle delays were assessed to be sufficiently long based on a comparison to a spectrum of a representative sample collected with a longer recycle delay to that used in this study and the absence of selective observation under such conditions.

Table 1. NMR Experimental Parameters

nucleus	f (MHz)	$\pi/2$ pulse width (μs)	a_t (ms)	d_1 (s)	reference (0 ppm)
^{17}O	115.190	15	30	0.05	D_2O[a]
^{43}Ca	57.184	50	30	0.3	1 M $CaCl_2$ in D_2O
^{67}Zn	53.166	50	30	0.3	1 M $Zn(NO_3)_2$ in D_2O

[a]The ^{17}O chemical shift of H_2O is 2.9 ppm with respect to D_2O (0 ppm).

A single-pulse sequence with an excitation pulse corresponding to a 45° tip angle was employed for each acquisition. The total data acquisition time for each experiment varied from a few hours to as long as 3 days, depending on the linewidth of the peaks, the sample concentration, and the sensitivity of the nuclei. All NMR measurements were carried out at room temperature (20 °C).

Quantum Chemistry Calculations

Computational modeling of the NMR chemical shifts (DFT-NMR) was carried out using the Amsterdam Density Functional (ADF-2018) package.[27] Geometries were optimized using the generalized gradient approximation applied to the Becke–Lee–Yang–Parr[28,29] functional. Calculations were carried out by using the all-electron TZ2P basis set (triple-ζ, 2-polarization function) with Slater-type orbitals[30] implemented in the ADF program. Cluster formation energies were estimated at the same level of theory taking the 0 K DFT energy of the cluster and subtracting the energy of the ion/molecular constituents in vacuum. Though clusters were optimized in a vacuum, explicit solvents near the cation of interest were employed as a reasonable first approximation.[31] NMR chemical shielding calculations were performed based on the geometry-optimized structures at the same level of theory and with the same basis set for each atom. To convert the calculated shielding to the experimentally observed scale, a reference shielding for each nucleus (^{43}Ca, ^{67}Zn, or ^{17}O) was established in accordance with the use of experimental references of 1.0 M $CaCl_2$ in D_2O for ^{43}Ca, 1.0 M $Zn(NO_3)_2$ in D_2O for ^{67}Zn, and D_2O for ^{17}O, respectively. The Ca^{2+} in 1.0 M $CaCl_2$ and Zn^{2+} in 1.0 M $Zn(NO_3)_2$ are fully solvated by water molecules. Solvation numbers ranging from 6 to 27 water molecules were examined as solvation shells around each Ca^{2+} or Zn^{2+}, and the geometries were optimized before NMR calculations. For all the calculations, the first solvation shell of the cation relaxed to contain six water molecules to form an octahedral coordination with the remaining water molecules entering into the second or third solvation shell. With the increase of water molecules from 6 to 27, the calculated ^{43}Ca chemical shielding progressively decreased. Regression analysis of the chemical shielding as a function of the number of water molecules reveals a ^{43}Ca chemical shielding approaching 1093 ppm when a Ca^{2+} is solvated by infinite number of water molecules. Thus, the equation $\delta_{obs} = 1093 - \delta_{calc}$ was used to convert the calculated ^{43}Ca chemical shielding to the experimentally observed scale with reference to 1.0 M $CaCl_2$ in D_2O. Detailed descriptions of the relationship between ^{43}Ca (^{67}Zn) chemical shielding and the number of solvating H_2O molecules is provided in Supporting Information Figures S1–S3 and Table S1. Note that the current NMR calculations do not differentiate between H and D isotopes of hydrogen. For ^{67}Zn, the calculated shielding values for Zn^{2+} solvated by 10, 12, and 20 water molecules are similar, that is, 1789.6 ppm for 10 H_2O, 1788.3 ppm for 12 H_2O, and 1785.8 ppm for 20 H_2O. Given the non-continuous changes in the shift from 4 to 20 waters, the average of these three tight clusters (1788 ppm) is taken as the reference. In fact, the average shielding of Zn^{2+} with 4, 6, 10, 12, 16, and 20 H_2O is 1784.9 ppm, which is very close to 1788 ppm, supporting this decision. To convert the calculated shielding to the experimentally observed ^{67}Zn chemical shift scale with reference to 1.0 M $Zn(NO_3)_2$, the following equation is used: $\delta_{obs} = 1788 - \delta_{calc}$. Similarly, for the ^{17}O chemical shift reference, clusters containing up to 14 H_2O molecules were used to simulate the effect of the hydrogen bonding network, and the chemical shift of the center-most oxygen was used since it experiences the effects of the simulated hydrogen bonding network (averaging with those on the outside of the cluster would skew the results). The following equation was found valid to convert the calculated shielding to the experimentally observed ^{17}O chemical shift scale with reference to pure water: $\delta_{obs} = 247.8 - \delta_{calc}$.

A variety of solvation models for Ca^{2+} or Zn^{2+} containing zero to two $TFSI^-$ anions (+2 to neutral cluster charge) and zero to six 2-MeTHF or THF molecules were relaxed, and then the ^{17}O and ^{43}Ca or ^{67}Zn chemical shifts were evaluated. The models are proposed based on the Ca^{2+} or Zn^{2+} cation coordinating with the oxygen atoms in the systems, with each $TFSI^-$ offering two coordination sites (bidendate) to a divalent cation, while each solvent molecule offers one coordination site since there is only one oxygen atom in each molecule of either THF or 2-MeTHF. This ansatz covers the range of possible coordination numbers from 4 to 6. A coordination number of 4 is based on the nominal formula of bidentate $Ca(TFSI)_2$ or $Zn(TFSI)_2$, whereas the coordination number 6 is the maximum coordination that Zn^{2+} will likely accept and is the experimentally observed value for Ca^{2+} as X-ray absorption spectroscopy (XAS) measurements suggest in solutions with THF.[32] Specifically, the following four types of models are used (see Scheme 1). Type-1: a fully solvated Ca^{2+} (or Zn^{2+}) cation that is coordinated by four to six THF (or 2-MeTHF) molecules; type-2: a $Ca(TFSI)^+$ or $Zn(TFSI)^+$) CIP cation with bidentate anion coordination and two to four solvent molecules; type-3: neutral $Ca(TFSI)_2$ or $Zn(TFSI_2)$ with one or two solvent molecules; and type-4: a CIP in which the cation expresses monodentate anion coordination and four solvent molecules (based on a recent report showing a monodentate TFSI coordination structure of Mg^{2+}).[33] The predicted ^{17}O, ^{43}Ca, and ^{67}Zn chemical shifts are listed in Table S2. Note that during geometry optimization,

https://doi.org/10.1021/jacsau.2c00046
JACS Au 2022, 2, 917–932

Scheme 1. Pictorial Representations of the Four Types of Models Utilized

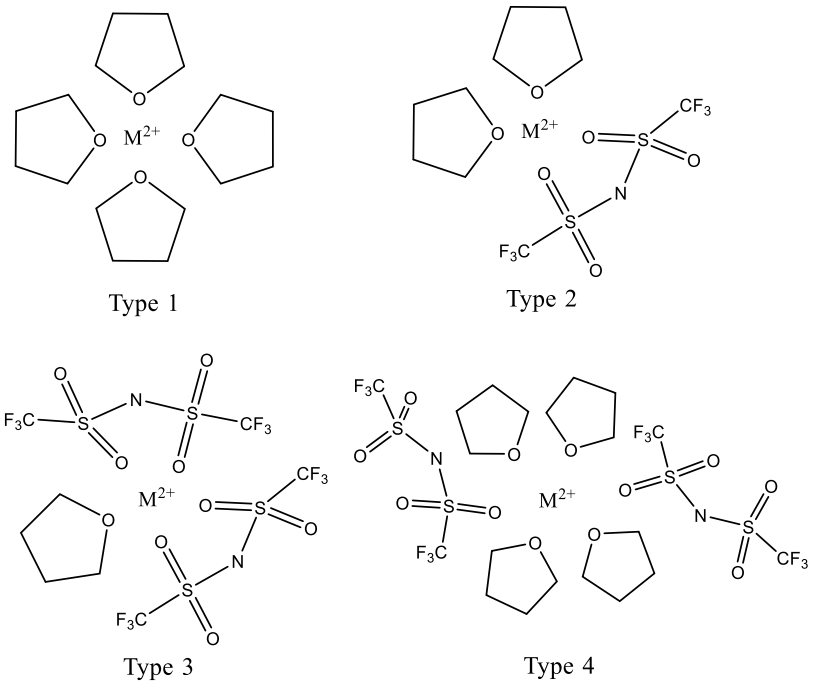

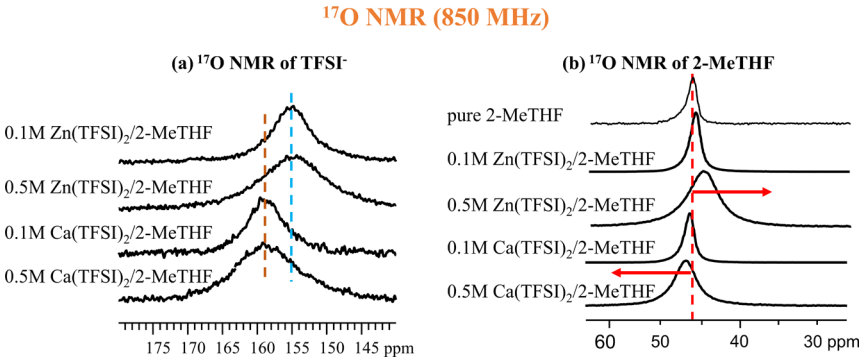

Figure 1. ^{17}O NMR spectra (with reference to D_2O) of the $TFSI^-$ anion (a) and the 2-MeTHF solvent (b) in electrolytes with two concentrations (0.1 and 0.5 M) of $Ca(TFSI)_2$ and $Zn(TFSI)_2$ in 2-MeTHF, showing the increased line broadening of both the anions and the solvents at an increased concentration and the trend of the chemical shifts related to the two different cations.

no restrictions are applied, that is, the geometries of each model are fully optimized and successfully converged.

RESULTS AND DISCUSSION

Experimental Results

Analysis of Anion and Solvent Environments by ^{17}O NMR. Both $Zn(TFSI)_2$ and $Ca(TFSI)_2$ are highly soluble in 2-MeTHF, yet these solutions differ in ionic conductivity by nearly an order of magnitude, with $Zn(TFSI)_2$ having a greater conductivity than $Ca(TFSI)_2$.[19] To understand the origin of this difference from a fundamental solvation perspective, two samples, of both salts in 2-MeTHF, with concentrations of 0.1 and 0.5 M, were investigated using ^{17}O NMR to interrogate both the anion−cation and solvent−cation interactions.

Evidence of a Fast Molecular Exchange. A single ^{17}O NMR peak is observed for the $TFSI^-$ anion at each salt concentration for both the Ca^{2+} and Zn^{2+} solutions, indicating a significant random molecular motion (including rotation, vibration, segmental motion, and reorientation of the molecule) associated with the $TFSI^-$ anion at a time scale much faster than the NMR time scale of milliseconds. Such a random molecular motion results in an average of the observed chemical shift of the four oxygen atoms in a $TFSI^-$ anion, generating a single peak. This further indicates that the exchange of $TFSI^-$ into and out of the M^{2+} (Ca^{2+} or Zn^{2+}) solvation shell is relatively rapid. A single ^{17}O peak is also obtained for the solvent 2-MeTHF. Based on quantum chemistry analysis (vide infra), some of the 2-MeTHF molecules are bound to the cation (M = Ca^{2+} or Zn^{2+}) to form the solvation shell around the cations, while most of the solvent molecules are free of cationic interactions owing to the much larger pool of 2-MeTHF relative to that of $M(TFSI)_2$ for the given salt concentrations investigated. A single solvent ^{17}O NMR peak provides strong evidence that there is extensive molecular exchange between the bound and the free solvent molecules with a time scale much faster than the NMR time scale of milliseconds. Such a quick exchange motion also averages out the chemical shift difference among the various bonded positions to the cations, reflecting a chemical shift that favors that of the free molecules due to their relative

https://doi.org/10.1021/jacsau.2c00046
JACS Au 2022, 2, 917−932

abundance. The importance of such a molecular exchange is twofold: (a) creating an opportunity for the cations to move much more efficiently across space, that is, self-diffusion in the absence of an electric field and migration between the anode and the cathode during the charge−discharge process in the presence of an electrical field and (b) creating an opportunity for the cations to be de-solvated/re-solvated at the electrode interfaces.

Evidence of CIP. Since the ^{17}O chemical shift for a $TFSI^-$ anion solvated by each solvent alone should be the same for both the cases of Ca^{2+} and Zn^{2+} in the absence of cation interactions, their disparities (Figure 1a) provide strong evidence of CIP formation between $TFSI^-$ and either cation. Indeed, contact ion pairing has been demonstrated for both $Ca(TFSI)_2$ and $Zn(TFSI)_2$ in 2-MeTHF through Raman spectroscopy, suggesting relatively weak solvent−cation interactions.[17,19] However, solvent-shared ion pairs (SIPs) may still be present in addition to the CIPs. To verify this possibility, DFT-NMR calculations were conducted. It was found that SIPs are indeed possible for the system of $THF_6Ca(TFSI)^+$ and $THF_6Zn(TFSI)^+$ where the first solvation shell contains six THF molecules with the oxygen atom from each THF coordinated to Ca^{2+} and where the first solvation shell to Zn^{2+} can have either five or six THF molecules. The corresponding models are depicted in Scheme S1.

Cation Size Effects and Spectroscopic Criteria/Evidence for Identifying Solvation Structures. For the 0.1 M and the 0.5 M $Ca(TFSI)_2$ salt concentrations, the linewidth of the ^{17}O peak associated with $TFSI^-$ is significantly broadened at a 0.5 M concentration compared with that of 0.1 M (1157 Hz for 0.5 M *vs* 658 Hz for 0.1 M), while the peak centers for the $TFSI^-$ anion are only slightly different (*i.e.*, 159.3 for 0.1 M and 159.7 ppm for 0.5 M) (Figure 1 and Table 2). Similar results are obtained for the case of $Zn(TFSI)_2$.

Table 2. Experimental ^{17}O Chemical Shifts

sample	$TFSI^-$ ppm ($\Delta\nu_{1/2}$ Hz)	THF ppm ($\Delta\nu_{1/2}$ Hz)	2-MeTHF ppm ($\Delta\nu_{1/2}$ Hz)
pure THF		19.5 (135)	
pure 2-MeTHF			46.65 (156)
0.1 M $Ca(TFSI)_2$/THF	159.3 (658)	19.3 (128)	
0.5 M $Ca(TFSI)_2$/THF	159.7 (1157)	20.2 (237)	
0.1 M $Ca(TFSI)_2$/2-MeTHF	159.1 (968)		46.5 (169)
0.5 M $Ca(TFSI)_2$/2-MeTHF	159.1 (1127)		47.1 (480)
0.8 mM $Zn(TFSI)_2$/THF		19 (213)	
4 mM $Zn(TFSI)_2$/THF	160 (580)	19 (215)	
0.1 M $Zn(TFSI)_2$/2-MeTHF	154.78 (760)		46.2 (176)
0.5 M $Zn(TFSI)_2$/2-MeTHF	154.2 (1270)		45.2 (540)

However, relative to the Ca^{2+} system, the ^{17}O chemical shift of $TFSI^-$ in the Zn system is shifted upfield by about 5 ppm, that is, at 154.78 ppm for the 0.1 M and 154.2 ppm for the 0.5 M $Zn(TFSI)_2$, respectively, indicating a strong cation size effect that we propose impacts the observed ionic conductivity trends. Complementary information on the bonding status of the solvent can be directly obtained from the ^{17}O NMR spectra of 2-MeTHF. Relative to pure 2-MeTHF, the ^{17}O peak center gradually shifts upfield (*i.e.*, decreasing shift values) with an increasing salt concentration for Zn^{2+}, while an opposite peak shift trend is obtained in the case of Ca^{2+} (Figure 1b). This distinct and opposite ^{17}O NMR shift behavior for Ca^{2+} and Zn^{2+} provides another unique criterion for establishing concrete pictures of the solvation structures of cations (Ca^{2+} and Zn^{2+}) using quantum chemistry (DFT-NMR) calculations.

Structure-Directing Roles of the Cation Size and the Solvent. While the solubility of $Ca(TFSI)_2$ is similar in either THF or 2-MeTHF (≥0.5 M), the solubility of $Zn(TFSI)_2$ is dramatically lower in THF (~0.004 M). Since solubility quantifies the equilibrium state achieved when the rate of dissolution (or solvation) equals the rate of precipitation, the large difference in solubility between the two salts in THF indicates a strong cation size effect on solvation structures and dynamics. The ^{17}O NMR spectra provide insight into this relationship. It is shown in Figure S4a (Supporting Information) that the center of the $TFSI^-$ ^{17}O peak for $Ca(TFSI)_2$ in THF is located at about 159.3 (0.1 M) and 159.7 ppm (0.5 M). These chemical shifts are similar to those of $Ca(TFSI)_2$ in 2-MeTHF, which indicates a similar chemical environment and perhaps a similar solvation structure in either solvent. Furthermore, the 4 mM $Zn(TFSI)_2$ in THF exhibits a $TFSI^-$ peak center at a similar value to that of $Ca(TFSI)_2$, indicating a similar $TFSI^-$ chemical environment in THF regardless of the cation. However, this chemical shift is about 5 ppm downfield from the ^{17}O peak measured for $Zn(TFSI)_2$ in 2-MeTHF (Figure 1a), indicating that the solvent has a profound effect on the Zn^{2+}−$TFSI^-$ coordination structure. Therefore, the large solubility difference for $Zn(TFSI)_2$ in THF versus 2-MeTHF is correlated to this structure difference. It should be pointed out that this is the first time an ^{17}O peak for $TFSI^-$ can be detected at a salt concentration as low as 4 mM and at a natural ^{17}O abundance. We attempted a similar experiment using a solution with a 0.8 mM $Zn(TFSI)_2$ concentration in THF; however, no $TFSI^-$ ^{17}O peak could be detected after a couple of days of continuous data acquisition even using a high field and large sample volume. It is also noted that the peak center for 4 mM $Zn(TFSI)_2$ in THF is essentially the same as that of the pure solvent THF due to the negligible number of Zn^{2+} solvation shells in solution.

Analysis of M^{2+} Environments by ^{43}Ca and ^{67}Zn NMR

Relative Exchange Dynamics. A single narrow ^{43}Ca NMR peak is observed for $Ca(TFSI)_2$ in both THF and 2-MeTHF, with chemical shifts/half linewidths displayed in Table 3 for 0.1 and 0.5 M $Ca(TFSI)_2$ in THF as well as 0.1 and 0.5 M $Ca(TFSI)_2$ in 2-MeTHF (see Figure 2). There are two explanations which can describe the observed single and very narrow ^{43}Ca peak; (1) a unique coordination structure

Table 3. Experimental ^{43}Ca and ^{67}Zn Chemical Shifts

sample	^{43}Ca ppm ($\Delta\nu_{1/2}$ Hz)	^{67}Zn ppm ($\Delta\nu_{1/2}$ Hz)
1 M $CaCl_2$	0 (62)	
0.1 M $Ca(TFSI)_2$/THF	−19.8 (40)	
0.5 M $Ca(TFSI)_2$/THF	−19.1 (49)	
0.1 M $Ca(TFSI)_2$/2-MeTHF	−22.3 (47)	
0.5 M $Ca(TFSI)_2$/2-MeTHF	−22.5 (52)	
1 M $Zn(NO_3)_2$		0 (85)
0.1 M $Zn(TFSI)_2$/2-MeTHF		−50.5 (1273)
0.5 M $Zn(TFSI)_2$/2-MeTHF		−50.2 (1836)

https://doi.org/10.1021/jacsau.2c00046
JACS Au 2022, 2, 917−932

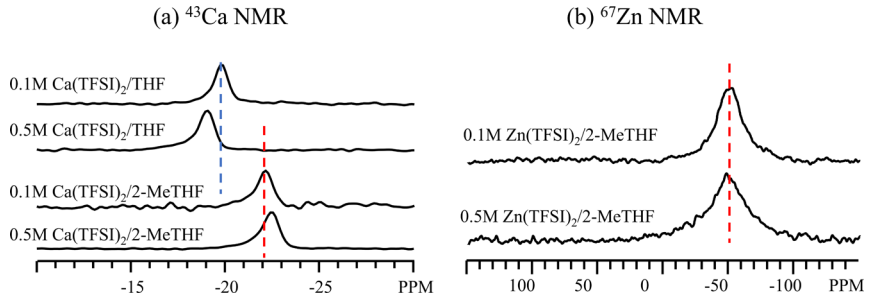

Figure 2. (a) ^{43}Ca NMR spectra of 0.1 and 0.5 M $Ca(TFSI)_2$ in THF and 2-MeTHF. (b) ^{67}Zn NMR spectra of 0.1 and 0.5 M $Zn(TFSI)_2$ in 2-MeTHF. Note that it is not possible to obtain ^{67}Zn NMR spectra of the 0.8 and 4 mM $Zn(TFSI)_2$ in THF due to poor sensitivity at such low concentrations of Zn^{2+}.

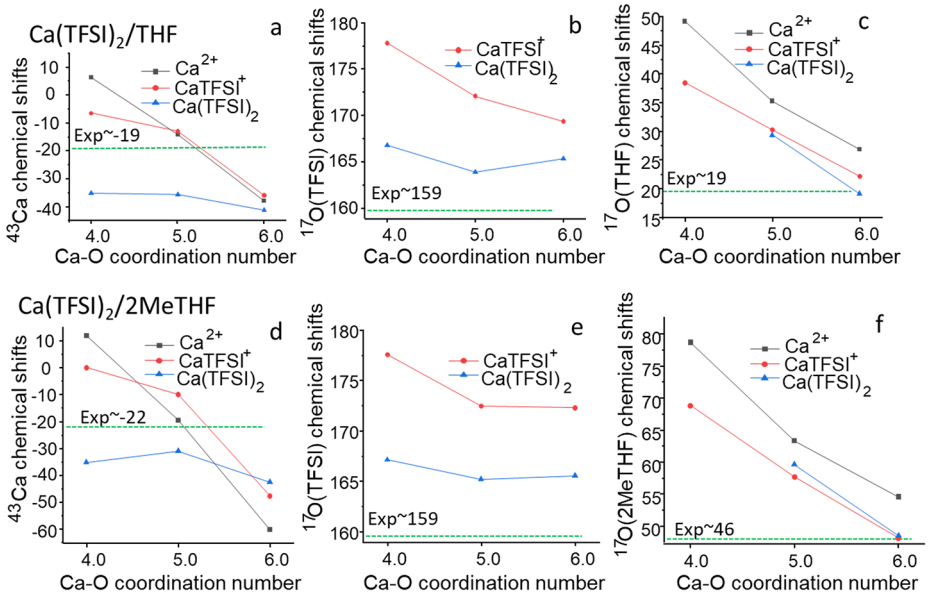

Figure 3. Quantum-chemistry-predicted ^{43}Ca and ^{17}O chemical shifts from the various solvation structures of $Ca(TFSI)_2$ dissolved in THF (a–c) and 2-MeTHF (d–f), respectively. In the legend, "Ca^{2+}" indicates a Ca^{2+} cation coordinated by only solvents, either THF (a–c), or 2-MeTHF (d–f). "$Ca(TFSI)^+$" represents a bidentate contact Ca^{2+}–$TFSI^-$ ion pair that is coordinated by different numbers of solvent molecules. "$Ca(TFSI)_2$" is for a neutral molecule that is coordinated by solvents, representing the case of solvents in salt. The horizontal dotted line represents the experimentally observed chemical shift. The structure for each cluster and coordination number can be found in Table S2, where the coordination numbers are given.

around Ca^{2+} with extremely high symmetry plus fast molecular motion and (2) fast time averaging among several unique coordination structures plus fast random molecular motion. In the second case, the Ca^{2+} must be highly mobile through space or fast solvent rearrangements are taking place. Due to the significant interactions of both $TFSI^-$ and solvent molecules with Ca^{2+}, its environment is not likely to be extremely symmetric as will be clear later in the discussion of the quantum chemistry results, suggesting that the second explanation is more reasonable. In contrast to Ca^{2+}, a much broader (relative to the reference solutions as shown in Figure S5) ^{67}Zn NMR peak is observed for $Zn(TFSI)_2$ in 2-MeTHF. This linewidth increases significantly with a concentration from 1273 Hz (0.1 M) to 1836 Hz (0.5 M), suggesting more diverse Zn^{2+} coordination structures and/or with decreased time averaging between these solvation structures (*i.e.*, slower exchange). Such a slower exchange for Zn^{2+} compared to Ca^{2+} could be explained by differences in cation charge density and apparent solvent and anion binding strength. The relatively smaller linewidth changes of ^{43}Ca and ^{67}Zn relative to ^{17}O with increasing concentration may be due to ^{17}O being more sensitive to the surrounding environment due to the presence of ionic and covalent interactions. Higher concentrations restrict the movement of electrolyte constituents and such a restriction is more obvious for ^{17}O species.

Relative Solvation Interactions. Aside from the slight increase in linewidth at a higher concentration, it is interesting to note that relative to those in THF, the ^{43}Ca peaks in 2-MeTHF are clearly shifted upfield by more than 2 ppm and the difference increases at increased salt concentrations. Furthermore, the ^{43}Ca peak center moves in the opposite direction with THF as opposed to 2-MeTHF, highlighting the effects of methyl group substitution. Previously, we found that the ionic conductivity of $Ca(TFSI)_2$ in THF is over 1 order of magnitude higher than in 2-MeTHF, presumably due to the decreased anion–cation interactions observed in the former.[19] The observed changes in the Ca^{2+} environment for THF versus 2-MeTHF, that is, Ca^{2+} is more shielded (manifested by a 2 ppm upfield shift) in 2-MeTHF than in THF, will offer great insights into the mechanisms that will be made clear in the

https://doi.org/10.1021/jacsau.2c00046
JACS Au 2022, 2, 917–932

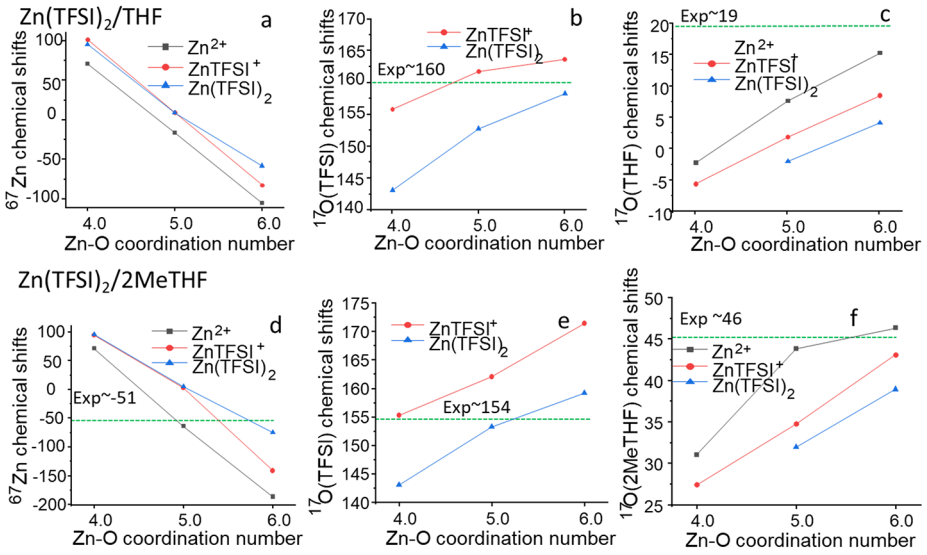

Figure 4. Quantum-chemistry-predicted ^{67}Zn and ^{17}O chemical shifts from the various solvation structures of $Zn(TFSI)_2$ dissolved in THF (a–c) and 2-MeTHF (d–f), respectively. The meaning of the legend is as follows. "Zn^{2+}" indicates a Zn^{2+} cation that is coordinated by only solvents, either THF (a–c) or 2-MeTHF (d–f). "$ZnTFSI^+$" represents a bidentate contact Zn^{2+}–$TFSI^-$ ion pair that is coordinated by different numbers of solvent molecules. "$Zn(TFSI)_2$" denotes a neutral molecule that is coordinated by solvents, representing the case of solvents in salt. The horizontal dotted line represents the experimentally observed chemical shift. The structure for each cluster and coordination number can be found in Table S2, where the coordination numbers are given.

detailed discussion of the solvent methyl substitution effects later in this work. For ^{67}Zn, the peak center is essentially unchanged within the experimental error range for both the 0.1 and 0.5 M concentrations, that is, −50.5 ppm (0.1 M) and −50.2 ppm (0.5 M), suggesting that the average Zn^{2+} environment is less concentration-dependent and therefore less variable than that of Ca^{2+}. One might expect this variability to correlate with the de-solvation kinetics of these electrolytes, although no direct evidence for this is currently available.

Analysis of the Solvation Structure by Quantum Chemistry

Identification of Cation Solvation Structures. The impacts of the solvation structure on the predicted chemical shifts of the measured nuclei are shown in Figures 3 and 4 for Ca and Zn, respectively, for a variety of model systems (Table S2 and Scheme 1). For $Ca(TFSI)_2$ in THF, an increasing Ca–O coordination number from 4 to 6 results in an upfield chemical shift (decreased ppm) for ^{43}Ca, ^{17}O of THF, and ^{17}O of the $TFSI^-$ associated with the CIP of $Ca(TFSI)^+$.

The increased shielding for the cation is likely a reflection of the increased electron density imparted by the added coordination of Ca to O atoms. The decreased chemical shifts in ^{17}O may be due to the higher electron density as the molecules become more bound in a tighter configuration. Furthermore, for the same Ca–O coordination number, the neutral species—$Ca(TFSI)_2$—have the most upfield shifted chemical shifts for the cation, the anion, and the solvents. Some similar trends are observed for the cases of $Ca(TFSI)_2$ dissolved in 2-MeTHF, for example, decreased chemical shift values for the cation, the anion, and the solvents with increasing Ca–O coordination number. The oxygen within $TFSI^-$ associated with the neutral species of $Ca(TFSI)_2$ is upfield shifted compared with the cases of the CIP $CaTFSI^+$ (Figure 3b,e). Given the experimental values of ∼20 ppm (THF, of which a vast majority are free in solution), 160 ppm ($TFSI^-$) and −19 ppm (^{43}Ca) for ^{17}O in the case of $Ca(TFSI)_2$ dissolved in THF, the probable solvation structures, based on best agreement with experimental values, consist of CIPs solvated by four THF molecules, neutral species of $Ca(TFSI)_2$ with one and two THF molecules, and Ca^{2+} solvated by five and six THF molecules, for which several structures with contrasting charges and coordination environments have been proposed and compared on the basis of predicted chemical shift and cluster formation energy (see the Supporting Information for an additional description). Taking these factors into account enables the identification of solvation structures which match the observed chemical shift by preferring those with lower energies. The results clearly suggest that neutral clusters are the most prevalent species in solutions for $Ca(TFSI)_2$ in THF, a result consistent with those from Raman studies.[19]

For $Ca(TFSI)_2$ in 2-MeTHF, the experimental values were measured as ∼47 ppm (2-MeTHF), 160 ppm ($TFSI^-$), and −23 ppm (^{43}Ca). A neutral cluster of $Ca(TFSI)_2$ with two 2-MeTHF molecules would be the most abundant solvation species based upon the relatively low formation energy. Furthermore, the possibility of monodentate neutral $Ca(TFSI)_2$ solvation structures, where each $TFSI^-$ anion donates only one oxygen atom for the bonding with Ca^{2+}, derived from the study of Mg^{2+} systems,[33] has also been investigated with quantum chemistry calculations on models of $Ca(TFSI)_2$ coordinated with four solvent molecules of either THF or 2-MeTHF. Despite the agreement between predicted and observed values for ^{17}O and the low energies (−459 kcal/mol) of such a cluster, the $TFSI^-$ and Ca chemical shift values are still 10–20 ppm disparate, so it is also possible that Ca with a coordination number of 5 provides the best overall agreement (−458 kcal/mol for THF). The possible solvation structures justified by quantum chemistry calculations based on the best agreement with experimental results are summarized in Table 4. It is apparent that the solvation structures in the studied electrolytes may contain multiple structures, indicating the coexistence of a range of complex solvation structures in

https://doi.org/10.1021/jacsau.2c00046
JACS Au 2022, 2, 917–932

Table 4. Calculated Model Chemical Shift[a,b]

Structure	Model	δ $^{17}O_{TFSI}$	δ $^{17}O_{THF}$	δ ^{43}Ca or ^{79}Zn	Cluster Formation Energy (kcal/mol)/ Likelihood
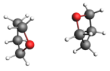	THF_2		24.055		-0.78
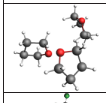	THF_3		20.12		-1
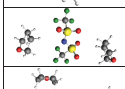	THF_2-TFSI	176.13	22.43		-6.2
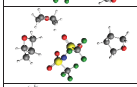	THF_3-TFSI	176.17	15.55		-8.1
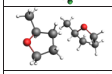	2-$MeTHF_2$		52.135		-0.4
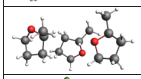	2-$MeTHF_3$		39.38		0.44
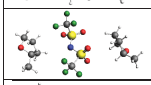	2-$MeTHF_2$-TFSI	176.26	49.42		-6.08
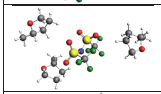	2-$MeTHF_3$-TFSI	174.6	42.6		-7.5
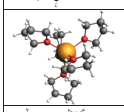	THF_5Ca^{2+}		35.346	-13.92	-259.5 P
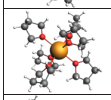	THF_6Ca^{2+}		26.972	-37.78	-277 P
	$THF_2Ca(TFSI)^+$	178.975	38.505	-6.35	-352.51 P
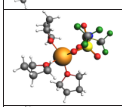	$THF_3Ca(TFSI)^+$	173.2225	30.32	-12.89	-374.9 P
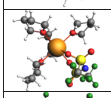	$THF_4Ca(TFSI)^+$	170.5225	22.275	-35.89	-391.1 P
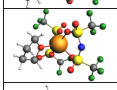	$THFCa(TFSI)_2$	165.045	29.43	-35.46	-439.8 L
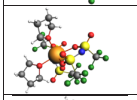	$THF_2Ca(TFSI)_2$	166.489	19.205	-41.03	-453.9 L
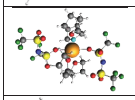	$THF_4Ca(TFSI)_2$ monodentate	173.265	29.1	-43.76	-458.8 MP, consistent with Raman[1]
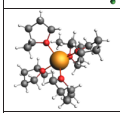	2-$MeTHF_5Ca^{2+}$		67.156	-19.28	-253.7 P
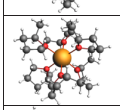	2-$MeTHF_6Ca^{2+}$		58.44	-60.01	-261.6 P
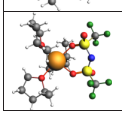	2-$MeTHF_3Ca(TFSI)^+$	173.2925	61.503	-9.83	-373.1 P

https://doi.org/10.1021/jacsau.2c00046
JACS Au 2022, 2, 917−932

Table 4. continued

Structure	Model	δ $^{17}O_{TFSI}$	δ $^{17}O_{THF}$	δ ^{43}Ca or ^{79}Zn	Cluster Formation Energy (kcal/mol)/ Likelihood
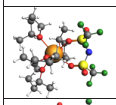	2-MeTHF$_4$Ca(TFSI)$^+$	173.14	51.9625	-47.42	-382.3 P
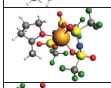	2-MeTHFCa(TFSI)$_2$	166.031	63.49	-30.84	-439.3 L
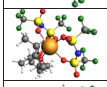	2-MeTHF$_2$Ca(TFSI)$_2$	166.391	52.395	-42.3	-452.2 MP, consistent with Raman[1]
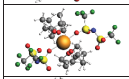	2-MeTHF$_4$Ca(TFSI)$_2$-monodendate	173.55	52.81	-58.65	-449.2 L
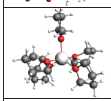	THF$_5$Zn^{2+}		7.634	-16.15	-374 P
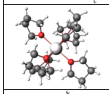	THF$_6$Zn^{2+}		15.262	-105.29	-381.7 P
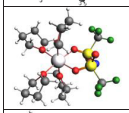	THF$_4$Zn(TFSI)$^+$	163.665	8.4925	-82.72	-499.7 P
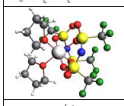	THF$_2$Zn(TFSI)$_2$	158.29	4.135	-57.92	-562.9 MP
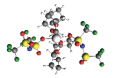	THF$_4$Zn(TFSI)$_2$-monodentate	166.6	16.8	-87.54	-563.4 MP, consistent with Raman[1]
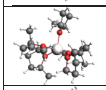	2-MeTHF$_5$Zn^{2+}		43.898	-63.39	-362.5 P
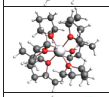	2-MeTHF$_6$Zn^{2+}		46.388	-185.33	-354.1 P
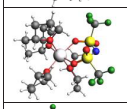	2-MeTHF$_4$Zn(TFSI)$^+$	171.51	43.1325	-140.33	-483.1 P
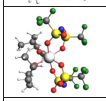	2-MeTHF$_2$Zn(TFSI)$_2$	159.284	38.98	-74.14	-559.8 MP, consistent with Raman[1]
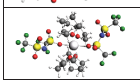	2-MeTHF$_4$Zn(TFSI)$_2$-monodendate	166.7	44.6	-138.27	-549.6 L

[a]Reported chemical shifts are average values among the chemically equivalent sites between different molecules due to fast exchange of the molecules in the models as explained in detail in the text. This table is a list of only likely solvation structures based on the agreement with the experimental values. Those highly likely are further emphasized. P—possible, L—likely, MP—most probable. [b]$\delta^{17}_{O} = 247.8 - \sigma_{calc}$, $\delta^{43}_{Ca} = 1093 - \sigma_{calc}$, $\delta^{79}_{Zn} = 1788 - \sigma_{calc}$.

the cases of Ca(TFSI)$_2$ dissolved in either THF or 2-MeTHF. Measured Raman spectra reveal noticeable differences in the TFSI$^-$ coordination structures of THF or 2-MeTHF that assist in identifying the most prevalent structures.[19] In particular, the reported line-shapes suggest that THF tends to allow a mixture of monodentate (slight blue shift) and bidentate (large blue shift) TFSI$^-$ populations, while 2-MeTHF primarily favors a bidentate population. This observation is consistent with the relative free energy differences found among the computed clusters from quantum chemistry and with the slightly different $^{17}O_{TFSI}$ chemical shift values in THF versus 2-MeTHF.

In contrast, for the cases of Zn(TFSI)$_2$ dissolved in THF or 2-MeTHF with increasing Zn−O coordination number, the ^{17}O chemical shifts of the TFSI$^-$ anion and the solvents shift downfield (increased chemical shift values), while the chemical shift of ^{67}Zn shifts upfield (decreased chemical shift values) for each of the three types of model solvation structures: Zn^{2+} solvated by solvents only, bidentate ZnTFSI$^+$ CIPs, and neutral species of Zn(TFSI)$_2$. This distinct difference with respect to the cases of Ca^{2+} highlights the cation size effect, whereby the larger Ca^{2+} cation yields ^{17}O chemical shifts of coordinating molecules, which are higher than those which do not coordinate. The larger cation size of Ca^{2+} means that smaller

https://doi.org/10.1021/jacsau.2c00046
JACS Au 2022, 2, 917−932

Table 5. Cation Size Effects: Calculated ^{17}O NMR Chemical Shifts of $TFSI^-$, 2-MeTHF, ^{43}Ca, and ^{67}Zn on Selected Solvation Structures[a,b]

Structure	Model	δ $^{17}O_{TFSI}$	δ $^{17}O_{THF}$	δ ^{43}Ca or ^{79}Zn	*Ca-O Zn-O distance (Å)	Formation energy
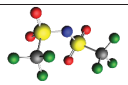	TFSI (CIS)	174.4				
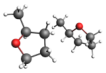	2-MeTHF$_2$		45.8 52.1			-0.4
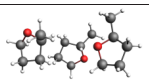	2-MeTHF$_3$		39.4			0.44
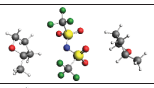	2-MeTHF$_2$-TFSI	176.3	49.4			-6.08
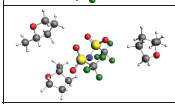	2-MeTHF$_3$-TFSI	175.5 174.6	46.1 42.6			-7.5
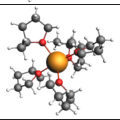	2-MeTHF$_5$Ca^{2+}		67.2	-19.3	2.405	-253.7 L
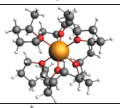	2-MeTHF$_6$Ca^{2+}		58.44	-60.01		-261.6 L
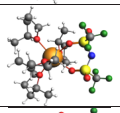	2-MeTHF$_4$Ca(TFSI)$^+$	173.14	51.9625	-47.42		-382 L
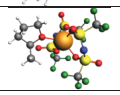	2-MeTHFCa(TFSI)$_2$	166.031	63.49	-30.84		-439.3 L
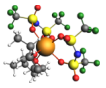	2-MeTHF$_2$Ca(TFSI)$_2$	166.4	52.4	-42.3	2.416 Ca-MeTHF 2.361 Ca-TFSI	-452.2 L
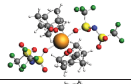	2-MeTHF$_4$Ca(TFSI)$_2$-monodendate	173.55	52.81	-58.65		−449.2 L
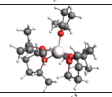	2-MeTHF$_5$Zn^{2+}		43.9	-63.4	2.173	-362.5 L
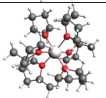	2-MeTHF$_6$Zn^{2+}		46.39	-185.33		-.54.2
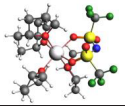	2-MeTHF$_4$Zn(TFSI)$^+$	171.51	43.13	-140.33		-483.1
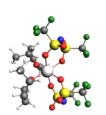	2-MeTHF$_2$Zn(TFSI)$_2$	159.3	39.0	-74.1	2.153 Zn-MeTHF 2.157 Zn-TFSI	-559.8 L
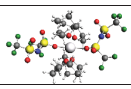	2-MeTHF$_4$Zn(TFSI)$_2$-monodendate	166.7	44.6	-138.27		-549.6

[a]P—possible, L—likely, MP—most probable. [b]Average distance between the cation and the bonded oxygen.

https://doi.org/10.1021/jacsau.2c00046
JACS Au 2022, 2, 917−932

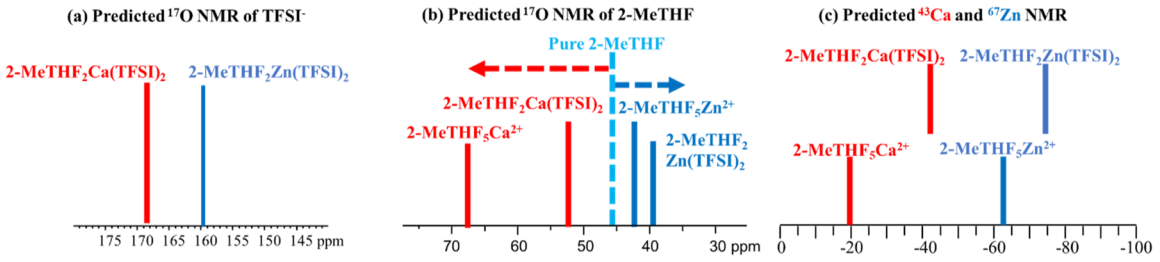

Figure 5. Quantum-chemistry-predicted ^{17}O, ^{43}Ca, and ^{67}Zn chemical shifts in solvation structures of 2-MeTHF$_5$Ca^{2+}/2-MeTHF$_5$Zn^{2+} and 2-MeTHF$_2$Ca(TFSI)$_2$/2-MeTHF$_2$Zn(TFSI)$_2$.

coordination numbers retain a significant distance between the molecules in the first solvation shell, resulting in a net deshielded ^{17}O nucleus, which becomes more shielded as the first solvation shell is populated. In contrast, the smaller Zn^{2+} cation is sufficiently small to shield the nucleus of ^{17}O beyond what occurs in a free solution, but the increasing Zn−O bond lengths at a higher coordination number deshields the nucleus to a greater extent than new shielding imparted by additional molecules in the first solvation shell. Given the experimental values of about 45 ppm (2-MeTHF), 154 ppm (TFSI$^-$), and −50 ppm (^{67}Zn) for Zn(TFSI)$_2$ dissolved in 2-MeTHF, the most probable solvation structures, based on the best agreement with experimental values, include CIPs solvated by four 2-MeTHF molecules, neutral Zn(TFSI)$_2$ solvated by two 2-MeTHF also with a Zn−O coordination number of 6, Zn solvated only by five 2-MeTHF molecules with a Zn−O coordination number of 5, and monodentate TFSI$^-$ neutral species with Zn(TFSI)$_2$ coordinated by four 2-MeTHF molecules, also with a Zn−O coordination number of 6. Since it is not presently possible to obtain ^{67}Zn NMR spectra on Zn(TFSI)$_2$ dissolved in THF due to the low solubility (4 mM and lower), no experimental shift is available to compare with computed values. Experimentally, we do know that the ^{17}O chemical shift of the TFSI$^-$ oxygen is located at about 154 ppm while that of the THF oxygen is at about 19 ppm, the latter of which is the same as from pure THF. This is quite reasonable as for a solution of 4 mM Zn(TFSI)$_2$ in THF, most of the THF molecules do not participate in the solvation structure of Zn^{2+} on the timescale of an NMR experiment. The weighted average of the chemical shifts will be nearly the same as that of pure THF assuming a fast molecular exchange between the Zn-bonded and the free THF molecules. Therefore, the criterion now relies on the ^{17}O chemical shift of 160 ppm to deduce the solvation structures. The most likely solvation structures are, therefore, the neutral bidentate Zn(TFSI)$_2$ species solvated by two THF molecules (Zn−O coordination number = 6), where the predicted chemical shifts are about 158 ppm (^{17}O in TFSI$^-$), 4 ppm (^{17}O in THF), and −58 ppm (^{67}Zn) and the monodentate Zn(TFSI)$_2$ with four THF molecules (Zn−O coordination number = 6), where the predicted chemical shifts are about 166 ppm (^{17}O in TFSI$^-$), 16.8 ppm (^{17}O in THF), and −87.5 ppm (^{67}Zn). It is thus apparent that the solvation structures of Zn(TFSI)$_2$ are unique to the solvents when comparing those in THF to those in 2-MeTHF, with THF containing predominantly monodentate and bidentate neutral species. This small number of structures may be the reason why the solubility of Zn(TFSI)$_2$ in THF is much lower than that in 2-MeTHF; the diversity of energetically favorable solvation structures increase the solubility in 2-MeTHF. The THF analogue also has a formation energy about 10 kcal/mol lower in magnitude than that of the 2-MeTHF solvated cluster, suggesting that it has a tighter binding. Further, these two structures also exhibit a relatively tighter binding compared to most other cluster models presented at −563 kcal/mol. The results suggest that monodentate TFSI coordination is preferred in THF while bidentate TFSI is preferred in 2-MeTHF, a result consistent with differences in the Raman spectra of these solutions in our previous works.[19] A possible explanation is that the monodentate configuration allows more THF molecules to coordinate to Zn^{2+} while 2-MeTHF is too bulky to derive such a benefit. It is worth considering why the monodentate-type structure could limit the solubility. Perhaps it favors aggregation by allowing the monodentate TFSI to bridge to other Zn^{2+} species. Table 4 summarizes the probable solvation structures for both Ca/Zn (TFSI)$_2$ in solvents of THF/2-MeTHF from this study.

Cation Size Effects. Insights into the cation size effects can now be obtained by comparing the cation−oxygen bond lengths in similar solvation structures between the cases of Ca^{2+} and Zn^{2+} in the solvent 2-MeTHF, where the only difference is the selection of Ca^{2+} or Zn^{2+}. The choice of 2-MeTHF for this discussion is due to the high cation concentration (>0.1 M) available for both Ca^{2+} and Zn^{2+} so that the metal cation NMR chemical shifts can be observed experimentally. Based on the best agreement with experimental values of ^{17}O shifts of TFSI$^-$ and 2-MeTHF as well as the ^{43}Ca and ^{67}Zn chemical shifts, the following two pairs of solvation structures can be identified for the comparison, that is, 2-MeTHF$_5$Ca^{2+}/2-MeTHF$_5$Zn^{2+}, where a cation is solvated by five 2-MeTHF molecules and 2-MeTHF$_2$Ca(TFSI)$_2$/2-MeTHF$_2$Zn(TFSI)$_2$, where a neutral salt species is solvated by 2-MeTHF molecules (Table 5).

The average ^{17}O chemical shift value of an isolated TFSI$^-$ is 174.4 ppm. When TFSI$^-$ is solvated by two to three 2-MeTHF molecules, the average ^{17}O chemical shift value for the TFSI$^-$ group is 175.5 ppm (Table 5), indicating a small contribution from the solvents that is primarily due to the longer distance between the solvent molecules and the TFSI$^-$ anion. It is found that the shortest distance between any one of the TFSI oxygen atoms and any one of the protons of 2-MeTHF is greater than 2.7 Å. Similarly, the calculated ^{17}O chemical shift for 2-MeTHF is at 46.1 ppm (Table 5), which is close to that of pure 2-MeTHF (45.8 ppm, Table 5), further validating the weak interaction between the solvent molecules of 2-MeTHF and TFSI$^-$ when a TFSI$^-$ is solvated by 2-MeTHF alone. The trend of the predicted chemical shifts for 2-MeTHF$_5$Ca^{2+}/2-MeTHF$_5$Zn^{2+} and 2-MeTHF$_2$Ca(TFSI)$_2$/2-MeTHF$_2$Zn(TFSI)$_2$ is summarized in Figure 5. The trends of the chemical shifts precisely match the experimentally observed trends shown in Figures 1 and 2, that is, the ^{17}O NMR chemical shifts

https://doi.org/10.1021/jacsau.2c00046
JACS Au 2022, 2, 917−932

Table 6. Solvent Effects (Methyl Substitution Effects): Calculated ^{17}O NMR Chemical Shifts of $TFSI^-$, THF, 2-MeTHF, and ^{43}Ca on Selected Solvation Structures

Structure	Model	δ $^{17}O_{TFSI}$		δ $^{17}O_{THF/2\text{-}MeTHF}$		δ ^{43}Ca	*Ca-O Zn-O distance	Formation energy
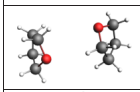	THF_2			22.1	24.1			-0.78
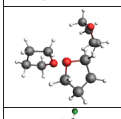	THF_3				20.1			-1
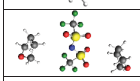	THF_2-TFSI	176.2	176.1	19.0	22.4			-6.2
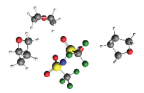	THF_3-TFSI		176.2		15.6			-8.1
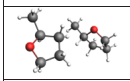	2-$MeTHF_2$			45.8	52.1			-0.4
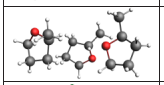	2-$MeTHF_3$				39.4			0.44
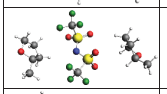	2-$MeTHF_2$-TFSI	175.5	176.3	46.0	49.4			-6.08
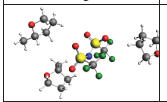	2-$MeTHF_3$-TFSI		174.6		42.6			-7.5
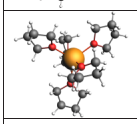	THF_5Ca^{2+}			35.3		-13.9	2.372	-259.5
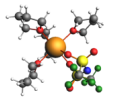	$THF_4Ca(TFSI)^+$	170.5		22.3		-35.9	Ca-THF 2.423 Ca-TFSI 2.363	-391.1
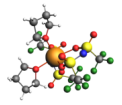	$THF_2Ca(TFSI)_2$	166.5		19.2		-41.0	Ca-THF 2.403 Ca-TFSI 2.355	-453.9
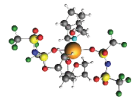	$THF_4Ca(TFSI)_2$-monodentate	173.3		29.1		-43.8	Ca-THF 2.429 Ca-TFSI 2.347	-458.8
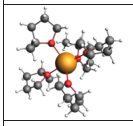	2-$MeTHF_5Ca^{2+}$			67.2		-19.3	2.405	-253.7
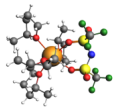	2-$MeTHF_4Ca(TFSI)^+$	173.1		52.0		-47.4	Ca-MeTHF 2.467 Ca-TFSI 2.377	-382
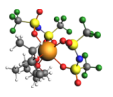	2-$MeTHF_2Ca(TFSI)_2$	166.4		52.4		-42.3	Ca-MeTHF 2.416 Ca-TFSI 2.361	-452.2
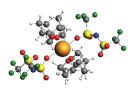	2-$MeTHF_4Ca(TFSI)_2$-monodendate	173.6		52.8		-58.7	Ca-MeTHF 2.475 Ca-TFSI 2.363	-449.2

https://doi.org/10.1021/jacsau.2c00046
JACS Au 2022, 2, 917−932

of the $TFSI^-$ associated with 2-$MeTHF_5Zn^{2+}$ shifted upfield compared to $TFSI^-$ with 2-$MeTHF_5Ca^{2+}$ (Figures 5a *vs* 1a), while the ^{17}O chemical shifts associated with the solvents of 2-MeTHF shifted upfield for the case of Zn^{2+} but shifted downfield for the case of Ca^{2+} (Figures 5b *vs* 1b) relative to pure 2-MeTHF. Furthermore, the chemical shift values of ^{67}Zn are also found to be more negative than those of ^{43}Ca, in excellent agreement with experimentally observed trends (Figures 5c *vs* 2). Significantly reduced bond distances (Table S4) and thus, a stronger bonding as suggested by the distances and confirmed by the formation energy of the cluster [−454 *vs* −560 kcal/mol for 2-$MeTHF_2Ca(TFSI)_2$ and 2-$MeTHF_2Zn(TFSI)_2$, respectively, see Supporting Information], between the coordinated oxygen atoms in both the solvents and $TFSI^-$, in the case of Zn^{2+}, are responsible for the experimentally observed chemical shift differences between the electrolytes of $Zn(TFSI)_2$ and $Ca(TFSI)_2$ in the studied cyclic ethers (Tables 3 and 4). For example, the average cation−O bond distance decreases from 2.405 Å for the case of 2-$MeTHF_5Ca^{2+}$, consistent with previous reports from XAFS of 2.41[17]−2.173 Å for 2-$MeTHF_5Zn^{2+}$. Such stronger interactions are reflected in the lower formation energy for the Zn cluster by nearly 110 kcal/mol. Similarly, for 2-$MeTHF_2Ca(TFSI)_2$, the average Ca−O bond distances are 2.416 Å for the coordinated Ca^{2+}-solvent O atoms and 2.361 Å for Ca^{2+}−$TFSI^-$, while for 2-$MeTHF_2Zn(TFSI)_2$, the corresponding bond distances decrease to 2.153 Å for the Zn^{2+}-solvent and 2.157 Å for Zn^{2+}−$TFSI^-$, respectively, with the 2-$MeTHF_2Zn(TFSI)_2$ cluster exhibiting an energy ∼110 kcal/mol lower. These combined energetic and bond distance analyses suggest that the anions bind more strongly to Zn^{2+} than to Ca^{2+}.

Solvent Effects. Solvent effects are evaluated by comparing the cation−oxygen bond lengths in similar solvation structures between the cases of Ca^{2+} in solvents of THF and 2-MeTHF. Ca^{2+} was selected since concentrations of 0.1 M and above can be achieved in both THF and 2-MeTHF solvents, and therefore the cation NMR chemical shifts can be obtained experimentally. Based on the best agreement with experimental values of the shifts of ^{17}O of $TFSI^-$, THF, and 2-MeTHF as well as the ^{43}Ca chemical shifts, the following three pairs of solvation structures are chosen for the comparison: 2-$MeTHF_5Ca^{2+}$/THF_5Ca^{2+} where a Ca^{2+} is solvated by five solvent molecules, 2-$MeTHF_2Ca(TFSI)_2$/$THF_2Ca(TFSI)_2$ where a neutral salt species is solvated by two solvents, and 2-$MeTHF_4Ca(TFSI)^+$/$THF_4Ca(TFSI)^+$ where a Ca^{2+}−$TFSI^-$ CIP is solvated by four solvent molecules (Table 6).

Theory predicts ^{17}O chemical shift values of 22.1 ppm for pure THF and 45.8 ppm for pure 2-MeTHF (Table 6) that are in excellent agreement with the experimental values of 19.5 ppm (THF) and 46.7 ppm (2-MeTHF). No significant difference in the ^{17}O chemical shifts is predicted by theory when a $TFSI^-$ anion is solvated by either THF (176.2 ppm) or 2-MeTHF (175.5 ppm), indicating that the interaction between the solvent molecules and the $TFSI^-$ anion is weak owing to the large distance between the $TFSI^-$ anion and THF. For 2-$MeTHF_5Ca^{2+}$/THF_5Ca^{2+}, 2-$MeTHF_2Ca(TFSI)_2$/$THF_2Ca(TFSI)_2$, and 2-$MeTHF_4Ca(TFSI)^+$/$THF_4Ca(TFSI)^+$, a general trend is predicted by theory that the ^{43}Ca resonances are upfield shifted for 2-MeTHF solvated models relative to those of THF. This trend agrees very well with the experimental observations shown in Figure 2a. The predicted ^{17}O NMR chemical shift of solvent molecules associated for each pair of solvation structures is upfield shifted by about 30 ppm for $CaTFSI^+$, which also agrees well with the experimentally observed trends (Table 2). Theory also predicts that the ^{17}O chemical shifts for $TFSI^-$ anions (Table 6), on the other hand, are not sensitive to the methyl substitution for each pair of solvation structures, also consistent with experimental observations (Table 1). A detailed evaluation of the solvation structure pairs reveals that the methyl substitution in the 2-position of THF causes an elongation of the bond between the Ca^{2+} and the coordinated oxygen atoms. Specifically, the average Ca−O bond distance increases from 2.372 Å for the case of THF_5 Ca^{2+} to 2.405 Å for 2-$MeTHF_5Ca^{2+}$(Table S5). This may also be reflected in the smaller formation energy of the substituted ether (2-MeTHF) solvate relative to THF (−534 *vs* −259 kcal/mol). Similarly, for $THF_2Ca(TFSI)_2$, the average Ca−O bond distances are 2.404 Å for the coordinated Ca^{2+}-solvent O atoms and 2.356 Å for Ca^{2+}−$TFSI^-$, while for 2-$MeTHF_2Ca(TFSI)_2$, the corresponding bond distances increase to 2.416 Å for the Ca^{2+}-solvent and 2.361 Å for Ca^{2+}−$TFSI^-$, respectively. Similar trends are observed for the cases of 2-$MeTHF_4Ca(TFSI)^+$/$THF_4Ca(TFSI)^+$. This demonstrates that 2-MeTHF exhibits a weaker interaction with Ca^{2+} than does THF, which explains the smaller amount of dissociated $TFSI^-$ observed through Raman spectroscopy in previous studies.[17,19] Furthermore, the shorter TFSI−Ca^{2+} bond distances than solvent−Ca^{2+} bond distances calculated in either solvent case confirm the relatively stronger interaction of $TFSI^-$ with Ca^{2+} compared to cyclic ether solvents. Based on the results from this work, a potential explanation for the previously reported enhanced ionic conductivity of $Ca(TFSI)_2$ in THF over 1 order of magnitude higher than in 2-MeTHF[19] is the smaller Ca^{2+} solvation cluster size associated with THF than that of 2-MeTHF rather than the decreased anion−cation interactions observed in the former. The smaller solvation cluster size facilitates efficient ion transfer and thus, enhanced ionic conductivity, assuming similar molecular dynamics in both solvents. Coupled with the higher percentage of free $TFSI^-$ anions in THF solvents based on Raman results, these two phenomena may account for an enhanced ionic conductivity.

Taken together, the solvation structures of $Ca(TFSI)_2$ in THF and 2-MeTHF are generally similar with the coexistence of several solvation structures. For $Ca(TFSI)_2$ in THF, the most probable first shell solvation structures include CIPs solvated by four THF molecules, that is, the $CaTFSI^+$ with six Ca−O coordinations, neutral species of $Ca(TFSI)_2$ with one and two THF molecules, and pure THF-solvated species of Ca^{2+} with five and six THF molecules. Combined with an analysis of the relative energies and previous findings, there appears to be some preference for neutral species of $Ca(TFSI)_2$ with one and two THF molecules. Methylating the THF molecule (2-MeTHF) in the Ca^{2+} system leads to probable solvation structures, with the coordination mimicking the THF system, that is, the $CaTFSI^+$ with six Ca−O coordinative bonds, neutral species of $Ca(TFSI)_2$ with two 2-MeTHF molecules, which is most probable, and pure 2-MeTHF solvated species of Ca^{2+} with six 2-MeTHF molecules. Monodentate $Ca(TFSI)_2$ structures are also possible solvation structures, where each $TFSI^-$ anion donates only one oxygen atom for the bonding with Ca^{2+} and is coordinated by four solvent molecules of either THF or 2-MeTHF. Solvent SIPs are possible for the species of $THF_6Ca(TFSI)^+$ and $THF_6Zn(TFSI)^+$ where the first solvation shell contains six THF molecules with the oxygen atom from each THF coordinated

https://doi.org/10.1021/jacsau.2c00046
JACS Au 2022, 2, 917−932

to Ca^{2+} and where the first solvation shell to Zn^{2+} can have either five or six THF molecules. Similarly, for $Zn(TFSI)_2$ dissolved in 2-MeTHF, the most probable solvation structures include CIPs solvated by four 2-MeTHF molecules, that is, the bidentate $CaTFSI^+$ with a Zn−O coordination number of 6, neutral $Zn(TFSI)_2$ solvated by two 2-MeTHF also with a Zn−O coordination number of 6, Zn solvated only by five 2-MeTHF molecules with a Zn−O coordination number of 5, and monodentate $TFSI^-$ neutral species with $Zn(TFSI)_2$ coordinated by four 2-MeTHF molecules. While multiple solvation structures are also found for the case of $Zn(TFSI)_2$ in 2-MeTHF, the solvation structures of $Zn(TFSI)_2$ in THF are more homogeneous, containing predominantly monodentate and bidentate neutral species. A comparison of similar solvation structures between Ca^{2+} and Zn^{2+} reveals a significant cation size effect that is manifested by the significantly reduced bond lengths between the cation and the coordinated oxygen atoms, that is, a stronger bonding to the cyclic ethers, for the cases of Zn^{2+} relative to Ca^{2+}. Significant solvent effects were also observed between the cases of THF and 2-MeTHF, where the methyl substitution was found to cause an elongation of the bonds between the cations and the coordinated oxygens atoms. The results from this study offer insights for electrolyte design in terms of efficient cation transfer and overall electrolyte stability. Efficient cation transfer can be achieved through a combination of the following attributes: (a) small solvation structures which promote fast movement of the solvated cation; (b) weak bonding of the cation with the anion and the solvent to promote fast ion exchange through space or *via* fast solvent/anion rearrangements; (c) weak interactions of the fully solvated cation cluster with the surrounding environment for fast movement of the solvated cation; (d) quick exchange of cations, anions, and solvent molecules among various possible solvated structures in the electrolytes if they coexist; and (e) stability of electrolytes in solution with the absence of decomposition at the electrode surface during cation desolvation-associated deposition and during resolvation of cations during the stripping of the electrochemical cycle. To this end, the tighter bonding observed for Zn^{2+} relative to Ca^{2+} may indicate a slower ion exchange and ionic diffusivity, and the methylated cyclic ethers may provide an improved electrochemical performance.

CONCLUSIONS

In this work, we have shown that the natural abundances ^{43}Ca, ^{67}Zn, and ^{17}O NMR provide a sufficiently sensitive strategy to gain structural information about solvation structures that can be accurately predicted with quantum chemistry DFT to offer detailed insights into solvation structures in electrolytes containing $Ca(TFSI)_2$ or $Zn(TFSI)_2$ in cyclic ether solvents of THF and 2-MeTHF. Based on the best multi-nuclear agreement between the theoretical and the experimentally observed chemical shifts and relative energetic comparisons, detailed solvation structures can be proposed and are supported when considering the formation energies of the clusters for a given cluster charge state. We show that selection of cations determines the strength of the metal−$O_{solvent}$ bonding environments for cyclic ethers in the electrolyte and that such a strength is consistent with what would be expected from the electronegativities and sizes of the ions. Methyl substitution on the cyclic ether solvents also leads to a weakening of the metal−$O_{solvent}$ bond, potentially due to steric hindrance effects. These properties have implications on ion transport during electrochemical cycling. The results also demonstrate fast molecular exchange on a time scale on the order of milliseconds among/between the various complex solvation structures through a combination of solvent rearrangements, cation exchange, molecular rotation, vibration, and so forth. Insights into the detailed solvation structures, including cation size and solvent effects, as well as apparent molecular dynamics, reveal the potential underlying explanations for solubility, and likely ion transport, which are fundamentally important for rational design of electrolytes in multivalent battery electrolyte systems, where improved performances are an ongoing central concern.

ASSOCIATED CONTENT

Supporting Information

The Supporting Information is available free of charge at https://pubs.acs.org/doi/10.1021/jacsau.2c00046.

Chemical shielding for dissolved cationic species; line broadening demonstrations for selected nuclei; additional description of theoretical calculations; additional computational modeling results; and DFT-optimized coordinates of all cluster models presented (PDF)

AUTHOR INFORMATION

Corresponding Authors

Jian Zhi Hu − *Joint Center for Energy Storage Research, Pacific Northwest National Laboratory, Richland, Washington 99352, United States; The Gene & Linda Voiland School of Chemical Engineering and Bioengineering, Washington State University, Pullman, Washington 99164, United States;* orcid.org/0000-0001-8879-747X; Phone: (509) 371-6544; Email: Jianzhi.Hu@pnnl.gov

Nathan T. Hahn − *Joint Center for Energy Storage Research, Material, Physical and Chemical Sciences Center, Sandia National Laboratories, Albuquerque, New Mexico 87185, United States;* orcid.org/0000-0001-6187-4068; Phone: (505) 844-8595; Email: nthahn@sandia.gov

Karl T. Mueller − *Joint Center for Energy Storage Research, Pacific Northwest National Laboratory, Richland, Washington 99352, United States;* orcid.org/0000-0001-9609-9516; Phone: (509) 371-6550; Email: Karl.Mueller@pnnl.gov

Authors

Nicholas R. Jaegers − *Joint Center for Energy Storage Research, Pacific Northwest National Laboratory, Richland, Washington 99352, United States;* orcid.org/0000-0002-9930-7672

Wenda Hu − *Joint Center for Energy Storage Research, Pacific Northwest National Laboratory, Richland, Washington 99352, United States; The Gene & Linda Voiland School of Chemical Engineering and Bioengineering, Washington State University, Pullman, Washington 99164, United States*

Kee Sung Han − *Joint Center for Energy Storage Research, Pacific Northwest National Laboratory, Richland, Washington 99352, United States;* orcid.org/0000-0002-3535-1818

Ying Chen − *Joint Center for Energy Storage Research, Pacific Northwest National Laboratory, Richland, Washington 99352, United States;* orcid.org/0000-0001-7417-0991

https://doi.org/10.1021/jacsau.2c00046
JACS Au 2022, 2, 917−932

Jesse A. Sears − *Joint Center for Energy Storage Research, Pacific Northwest National Laboratory, Richland, Washington 99352, United States*

Vijayakumar Murugesan − *Joint Center for Energy Storage Research, Pacific Northwest National Laboratory, Richland, Washington 99352, United States;* orcid.org/0000-0001-6149-1702

Kevin R. Zavadil − *Joint Center for Energy Storage Research, Material, Physical and Chemical Sciences Center, Sandia National Laboratories, Albuquerque, New Mexico 87185, United States;* orcid.org/0000-0002-3791-424X

Complete contact information is available at: https://pubs.acs.org/10.1021/jacsau.2c00046

Author Contributions

[‖]J.Z.H. and N.R.J. contributed equally.

Notes

The authors declare no competing financial interest.

■ ACKNOWLEDGMENTS

This work was supported by the Joint Center for Energy Storage Research (JCESR), an Energy Innovation Hub funded by the U.S. Department of Energy (DOE), Office of Science, Office of Basic Energy Sciences (BES). Experiments were conducted in the Environmental Molecular Sciences Laboratory (EMSL), a national scientific user facility sponsored by the Department of Energy's Office of Biological and Environmental Research at Pacific Northwest National Laboratory (PNNL). EMSL's supercomputers were utilized as a resource for computational modeling. PNNL is a multi-program national laboratory operated for DOE by the Battelle Memorial Institute under Contract DE-AC05-76RL01830. Sandia National Laboratories is a multimission laboratory managed and operated by National Technology & Engineering Solutions of Sandia, LLC, a wholly owned subsidiary of Honeywell International Inc., for the U.S. Department of Energy's National Nuclear Security Administration under contract DE-NA0003525. The authors acknowledge Nancy Washton for her support in improving the state of the large sample volume NMR probe. This paper describes objective technical results and analysis. Any subjective views or opinions that might be expressed in the paper do not necessarily represent the views of the U.S. Department of Energy or the United States Government.

■ REFERENCES

(1) Ponrouch, A.; Palacin, M. R. Post-Li batteries: promises and challenges. *Philos. Trans. R. Soc., A* **2019**, *377*, 20180297.

(2) Xu, W.; Wang, Y. Recent Progress on Zinc-Ion Rechargeable Batteries. *Nano-Micro Lett.* **2019**, *11*, 90.

(3) Luo, J.; Bi, Y.; Zhang, L.; Zhang, X.; Liu, T. L. A Stable, Non-Corrosive Perfluorinated Pinacolatoborate Mg Electrolyte for Rechargeable Mg Batteries. *Angew. Chem., Int. Ed.* **2019**, *58*, 6967−6971.

(4) Bitenc, J.; Pirnat, K.; Žagar, E.; Randon-Vitanova, A.; Dominko, R. Effect of salts on the electrochemical performance of Mg metal-organic battery. *J. Power Sources* **2019**, *430*, 90−94.

(5) Hu, J. Z.; Jaegers, N. R.; Chen, Y.; Han, K. S.; Wang, H.; Murugesan, V.; Mueller, K. T. Adsorption and Thermal Decomposition of Electrolytes on Nanometer Magnesium Oxide: An in Situ C-13 MAS NMR Study. *ACS Appl. Mater. Interfaces* **2019**, *11*, 38689−38696.

(6) Hu, J. Z.; Rajput, N. N.; Wan, C.; Shao, Y.; Deng, X.; Jaegers, N. R.; Hu, M.; Chen, Y.; Shin, Y.; Monk, J.; Chen, Z.; Qin, Z.; Mueller, K. T.; Liu, J.; Persson, K. A. Mg-25 NMR and computational modeling studies of the solvation structures and molecular dynamics in magnesium based liquid electrolytes. *Nano Energy* **2018**, *46*, 436−446.

(7) Goldman, J. L.; Mank, R. M.; Young, J. H.; Koch, V. R. Structure-Reactivity Relationships of Methylated Tetrahydrofurans with Lithium. *J. Electrochem. Soc.* **1980**, *127*, 1461.

(8) Aycock, D. F. Solvent Applications of 2-Methyltetrahydrofuran in Organometallic and Biphasic Reactions. *Org. Process Res. Dev.* **2007**, *11*, 156−159.

(9) Hattori, M.; Yamamoto, K.; Matsui, M.; Nakanishi, K.; Mandai, T.; Choudhary, A.; Tateyama, Y.; Sodeyama, K.; Uchiyama, T.; Orikasa, Y.; Tamenori, Y.; Takeguchi, T.; Kanamura, K.; Uchimoto, Y. Role of Coordination Structure of Magnesium Ions on Charge and Discharge Behavior of Magnesium Alloy Electrode. *J. Phys. Chem. C* **2018**, *122*, 25204−25210.

(10) Aurbach, D.; Lu, Z.; Schechter, A.; Gofer, Y.; Gizbar, H.; Turgeman, R.; Cohen, Y.; Moshkovich, M.; Levi, E. Prototype systems for rechargeable magnesium batteries. *Nature* **2000**, *407*, 724−727.

(11) Kim, H. S.; Arthur, T. S.; Allred, G. D.; Zajicek, J.; Newman, J. G.; Rodnyansky, A. E.; Oliver, A. G.; Boggess, W. C.; Muldoon, J. Structure and compatibility of a magnesium electrolyte with a sulphur cathode. *Nat. Commun.* **2011**, *2*, 427.

(12) Doe, R. E.; Han, R.; Hwang, J.; Gmitter, A. J.; Shterenberg, I.; Yoo, H. D.; Pour, N.; Aurbach, D. Novel, electrolyte solutions comprising fully inorganic salts with high anodic stability for rechargeable magnesium batteries. *Chem. Commun.* **2014**, *50*, 243−245.

(13) Kim, I.-T.; Yamabuki, K.; Sumimoto, M.; Tsutsumi, H.; Morita, M.; Yoshimoto, N. Characteristics of tetrahydrofuran-based electrolytes with magnesium alkoxide additives for rechargeable magnesium batteries. *J. Power Sources* **2016**, *323*, 51−56.

(14) Liu, T.; Shao, Y.; Li, G.; Gu, M.; Hu, J.; Xu, S.; Nie, Z.; Chen, X.; Wang, C.; Liu, J. A facile approach using MgCl2 to formulate high performance Mg2+ electrolytes for rechargeable Mg batteries. *J. Mater. Chem. A* **2014**, *2*, 3430.

(15) Liao, C.; Guo, B.; Jiang, D.-e.; Custelcean, R.; Mahurin, S. M.; Sun, X.-G.; Dai, S. Highly soluble alkoxide magnesium salts for rechargeable magnesium batteries. *J. Mater. Chem. A* **2014**, *2*, 581−584.

(16) Wang, D.; Gao, X.; Chen, Y.; Jin, L.; Kuss, C.; Bruce, P. G. Plating and stripping calcium in an organic electrolyte. *Nat. Mater.* **2018**, *17*, 16−20.

(17) Hahn, N. T.; Driscoll, D. M.; Yu, Z.; Sterbinsky, G. E.; Cheng, L.; Balasubramanian, M.; Zavadil, K. R. Influence of Ether Solvent and Anion Coordination on Electrochemical Behavior in Calcium Battery Electrolytes. *ACS Appl. Energy Mater.* **2020**, *3*, 8437−8447.

(18) Forero-Saboya, J. D.; Marchante, E.; Araujo, R. B.; Monti, D.; Johansson, P.; Ponrouch, A. Cation Solvation and Physicochemical Properties of Ca Battery Electrolytes. *J. Phys. Chem. C* **2019**, *123*, 29524−29532.

(19) Han, K. S.; Hahn, N. T.; Zavadil, K. R.; Jaegers, N. R.; Chen, Y.; Hu, J. Z.; Murugesan, V.; Mueller, K. T. Factors Influencing Preferential Anion Interactions during Solvation of Multivalent Cations in Ethereal Solvents. *J. Phys. Chem. C* **2021**, *125*, 6005−6012.

(20) Hu, J. Z.; Jaegers, N. R.; Hu, M. Y.; Mueller, K. T. In situ and ex situ NMR for battery research. *J. Phys.: Condens. Matter* **2018**, *30*, 463001.

(21) Jaegers, N. R.; Mueller, K. T.; Wang, Y.; Hu, J. Z. Variable Temperature and Pressure Operando MAS NMR for Catalysis Science and Related Materials. *Acc. Chem. Res.* **2020**, *53*, 611−619.

(22) Wan, C.; Hu, M. Y.; Borodin, O.; Qian, J.; Qin, Z.; Zhang, J.-G.; Hu, J. Z. Natural abundance 17 O, 6 Li NMR and molecular modeling studies of the solvation structures of lithium bis-(fluorosulfonyl)imide/1,2-dimethoxyethane liquid electrolytes. *J. Power Sources* **2016**, *307*, 231−243.

(23) Hu, M. Y.; Deng, X.; Thanthiriwatte, K. S.; Jackson, V. E.; Wan, C.; Qafoku, O.; Dixon, D. A.; Felmy, A. R.; Rosso, K. M.; Hu, J. Z. In Situ Natural Abundance 17O and 25Mg NMR Investigation of Aqueous Mg(OH)2 Dissolution in the Presence of Supercritical CO2. *Environ. Sci. Technol.* **2016**, *50*, 12373−12384.
(24) Deng, X.; Hu, M. Y.; Wei, X.; Wang, W.; Chen, Z.; Liu, J.; Hu, J. Z. Natural abundance 17 O nuclear magnetic resonance and computational modeling studies of lithium based liquid electrolytes. *J. Power Sources* **2015**, *285*, 146−155.
(25) Chen, Y.; Jaegers, N. R.; Wang, H.; Han, K. S.; Hu, J. Z.; Mueller, K. T.; Murugesan, V. Role of Solvent Rearrangement on Mg2+ Solvation Structures in Dimethoxyethane Solutions using Multimodal NMR Analysis. *J. Phys. Chem. Lett.* **2020**, *11*, 6443−6449.
(26) Chen, Y.; Jaegers, N. R.; Han, K. S.; Wang, H.; Young, R. P.; Agarwal, G.; Lipton, A. S.; Assary, R. S.; Washton, N. M.; Hu, J. Z.; Mueller, K. T.; Murugesan, V. Probing Conformational Evolution and Associated Dynamics of Mg(N(SO2CF3)(2))(2)center dot Dimethoxyethane Adduct Using Solid-State F-19 and H-1 NMR. *J. Phys. Chem. C* **2020**, *124*, 4999−5008.
(27) Baerends, E. J. A.; Berger, J. A.; Bérces, A.; Bickelhaupt, F. M.; Bo, C.; de Boeij, P. L.; Boerrigter, P. M.; Cavallo, L.; Chong, D. P.; et al. Amsterdam Density Functional. Theoretical Chemistry, Scientific Computing & Modelling (SCM), Theoretical Chemistry; Vrije Universiteit: Amsterdam, The Netherlands, URL: http://www.scm.com (accessed 1-1-2-21).
(28) Becke, A. D. Density-functional exchange-energy approximation with correct asymptotic behavior. *Phys. Rev. A* **1988**, *38*, 3098−3100.
(29) Lee, C.; Yang, W.; Parr, R. G. Development of the Colle-Salvetti Correlation-Energy Formula into a Functional of the Electron-Density. *Phys. Rev. B: Condens. Matter Mater. Phys.* **1988**, *37*, 785−789.
(30) Van Lenthe, E.; Baerends, E. J. Optimized Slater-Type Basis Sets for the Elements 1-118. *J. Comput. Chem.* **2003**, *24*, 1142−1156.
(31) Khetan, A.; Pitsch, H.; Viswanathan, V. Identifying Descriptors for Solvent Stability in Nonaqueous Li-O-2 Batteries. *J. Phys. Chem. Lett.* **2014**, *5*, 1318−1323.
(32) Driscoll, D. M.; Dandu, N. K.; Hahn, N. T.; Seguin, T. J.; Persson, K. A.; Zavadil, K. R.; Curtiss, L. A.; Balasubramanian, M. Rationalizing Calcium Electrodeposition Behavior by Quantifying Ethereal Solvation Effects on Ca2+ Coordination in Well-Dissociated Electrolytes. *J. Electrochem. Soc.* **2020**, *167*, 160512.
(33) Fan, S.; Asselin, G. M.; Pan, B.; Wang, H.; Ren, Y.; Vaughey, J. T.; Sa, N. A Simple Halogen-Free Magnesium Electrolyte for Reversible Magnesium Deposition through Cosolvent Assistance. *ACS Appl. Mater. Interfaces* **2020**, *12*, 10252−10260.

https://doi.org/10.1021/jacsau.2c00046
JACS Au 2022, 2, 917−932